Molecular Mie model for second harmonic generation and sum frequency generation

Sarina Wunderlich,[1,*,†] Benedikt Schürer,[2,*] Christian Sauerbeck,[2,*] Wolfgang Peukert,[2,*] and Ulf Peschel[1,*]

[1]*Institute of Optics, University of Erlangen-Nuremberg, Erlangen, Germany*

[2]*Institute of Particle Technology, University of Erlangen-Nuremberg, Erlangen, Germany*

(Received 4 August 2011; revised manuscript received 11 October 2011; published 1 December 2011)

A theoretical model to simulate second harmonic and sum frequency generation from stratified spherical particles of arbitrary material is presented and compared with the widely used Rayleigh-Gans-Debye approximation and to experimental results from polystyrene particles with adsorbed malachite green molecules. In this model, the nonlinear polarization is caused by individual dipoles placed in the vicinity of the sphere and is simulated on a molecular basis. This offers greater flexibility to model more sophisticated systems.

DOI: 10.1103/PhysRevB.84.235403 PACS number(s): 78.68.+m, 42.65.Ky, 42.25.Fx, 42.68.Mj

I. INTRODUCTION

Nonlinear light scattering, especially second harmonic generation, has been used from the 1980s on to study planar surfaces.[1,2] Second harmonic generation from the surface of nanospheres in suspension was first reported about a decade ago.[3,4] In the dipole approximation, second harmonic and sum-frequency generation are forbidden in the bulk of spheres of centrosymmetric materials as well as in the solvent itself making the method highly surface sensitive. It has been used in a wide range of applications to study the surface structure, adsorption and orientation of molecules to the surface of nanoparticles[3,5–14] or to determine the buried microstructure of particles,[15] to determine the size of particle clusters,[16] or in biophysical experiments as sensitive probing technique.[17–20]

The first theoretical model to calculate the second harmonic scattering from the surface of a metallic sphere was published by Agarwal and Jha.[21] for the limiting case of small particles. An exact solution in the Rayleigh limit ($R \ll \lambda$) has also been proposed by Dadap *et al.*, who calculated the vector potential from the current density source and expanded it in the small-particle limit into electric dipole and quadrupole and magnetic dipole moments. The first model took into account only the surface term and three $\chi^{(2)}$ components[22] but was soon expanded to all four $\chi^{(2)}$ components and a nonlocal bulk contribution.[23] This model was also used to model the nonlinear response of a sphere close to a surface,[24] of an array or composite of nanoparticles[25,26] or of particles interacting with focused beams.[27]

An exact solution for arbitrary particle sizes, based on Mie theory, was already proposed by Agarwal and Jha.[21] Östling *et al.*[28,29] published the first nonlinear Mie model for metallic spheres. They used an anharmonic oscillator model, which takes only the $\chi^{(2)}_{zzz}$ component into account, to calculate the second harmonic response.

Pavlyukh and Hübner[30] refined the nonlinear Mie model without restriction to an anharmonic oscillator model; instead the nonlinear polarization is calculated directly from $\chi^{(2)}$ and from the scattered electric fields at the surface of the sphere. The boundary conditions used to correlate the nonlinear polarization $\vec{P}_{2\omega}$, or the surface current $\vec{j}_s$, to the second harmonic fields $\vec{E}$ and $\vec{H}$ are (with $\vec{n}$ being the surface normal)

$$\vec{n} \times (\vec{E}_{\text{out}} - \vec{E}_{\text{in}}) = 0,$$

$$\vec{n} \times (\vec{H}_{\text{out}} - \vec{H}_{\text{in}}) = \vec{j}_s = -2i\delta\omega\vec{n} \times (\vec{P}_{2\omega} \times \vec{n}).$$

They recognized three independent $\chi^{(2)}$ components at the surface, but restricted their solution to $\chi^{(2)}_{zzz}$.

De Beer and Roke[31] finally found the exact solution for four $\chi^{(2)}$ components. Using a reciprocity theorem, the problem of calculating the sum-frequency fields from the nonlinear polarization is traced back to the problem of calculating the fields inside the particle illuminated by a plane wave,[32] so that standard Mie scattering can be applied.

Gonella and Dai[33] expanded the exact solutions of Dadap and Shan[23] for a small particle size to a full Mie model. They used

$$\Delta\vec{E}_{\parallel}(2\omega) = -\frac{4\pi}{\epsilon'(2\omega)}\vec{\nabla}_{\parallel}P_{\perp}(2\omega),$$

$$\Delta\vec{H}_{\parallel}(2\omega) = 4\pi i\frac{2\omega}{c}\vec{n} \times \vec{P}(2\omega)$$

as boundary conditions.

The Rayleigh-Gans-Debye (RGD) or first Born approximation is quite likely the most common model to simulate the nonlinear response of nanoparticles because it requires less computational effort than all other known models. Here the refractive index of the sphere is assumed to be equal to that of the surrounding, so that the field of the fundamental harmonics is not influenced by the sphere and can be assumed to be a plane wave. The nonlinear polarization $\vec{P}$, oscillating at the sum frequency, which is driven by two fundamental harmonic fields (index 1 and 2), can then be determined in a straightforward way as

$$\vec{P}(\vec{r}) \propto \sum_{i,j,k=1}^{3} \vec{e}_i\chi^{(2)}_{ijk}E_{\text{FH},1}e^{i\vec{k}_{\text{FH},1}\vec{r}}(\vec{e}_{\text{FH},1} \cdot \vec{e}_j) \times E_{\text{FH},2}e^{i\vec{k}_{\text{FH},2}\vec{r}}(\vec{e}_{\text{FH},2} \cdot e_k),$$

where $\vec{k}_{\text{FH},1/2}$ and $\vec{e}_{\text{FH},1/2}$ are the wave vectors and polarization vectors of the two interacting fundamental harmonic (FH) fields, respectively. This polarization now itself induces an electric field at the sum frequency of the two fundamentals, which is radiated away as (compare to Brown,[34] where a different system of units is used)

$$\vec{E}(\vec{r}) = \frac{c^2}{4\pi\epsilon}\vec{\nabla} \times \vec{\nabla} \times \int d\vec{r}'\frac{e^{ik_{\text{SH}}|\vec{r}-\vec{r}'|}}{|\vec{r}-\vec{r}'|}\vec{P}(\vec{r}').$$

Again this approximation is only valid if the spheres do not influence the field propagation either due to index matching or due to a size, which is small compared with the wavelength ($\frac{2\pi R}{\lambda}|\frac{n_{\text{sph.}}}{n_{\text{surr.}}} - 1| \ll 1$). Usually the medium is additionally assumed to show no dispersion so that $|\vec{k}_{\text{SH}}| = 2|\vec{k}_{\text{FH}}|$. While Martorell *et al.* restricted their calculations to the $\chi^{(2)}_{zzz}$ component,[35] Roke, deBeer, and co-workers expanded the model to all relevant $\chi^{(2)}$ components[36,37] and also to nonspherical particles of arbitrary shape.[38] Viarbitskaya[39] even went a step further by developing a generalized nonlinear RGD theory, where also dispersion is taken into account.

Finally Roke[32] and Viarbitskaya[39] extended their simulation by applying the nonlinear Wentzel-Kramers-Brillouin model. Here the fundamental harmonic waves are still assumed to propagate without refraction but a phase factor proportional to the index contrast is taken into account. Still all these models lack a consistent description of the linear field propagation around the spheres.

Here, we report on a nonlinear Mie model, which correctly describes the field distributions both at the FH and SH frequencies. In contrast to previous Mie models, the polarization is directly modeled as a surface dipole density, applying the boundary conditions of Mie theory to the fields radiated from individual dipoles placed at the surface of the sphere. Our model does not rely on a homogeneous distribution of the nonlinear polarization at the surface of the sphere, which allows for situations where the polarization is not symmetric or not restricted to the surface of the sphere as might be the case for layers of molecules or for domains of molecules with varying orientation at the surface.

II. THEORY

A. System

We consider a sphere of radius R of a material with refractive index n_1 placed at the origin in a surrounding medium of refractive index n_2 (see Fig. 1).

The incident fundamental harmonic wave $\vec{E}_{\text{FH},1}$ is propagating along the Z axis of the global coordinate system, the second fundamental harmonic wave $\vec{E}_{\text{FH},2}$ in the X-Z plane with an angle θ_{FH} with respect to the Z axis. In the experiment the incident beam is usually polarized either parallel (p) or perpendicular (s) to the X-Z plane and the signal is detected in the X-Z plane as a function of the scattering angle θ with respect to the Z axis.

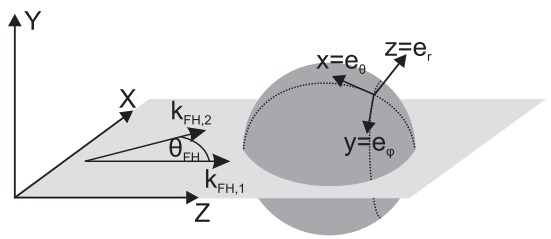

FIG. 1. Sphere with local coordinate system, global coordinate system at the surface of the sphere, and the wave vectors $\vec{k}_{\text{FH},1}$ and $\vec{k}_{\text{FH},2}$ of the incident beams.

The local coordinate system at the surface of the sphere is given by the spherical coordinate system, with $\vec{e}_x = \vec{e}_r$, $\vec{e}_y = \vec{e}_\theta$, and $\vec{e}_y = \vec{e}_\phi$.

B. Linear Mie scattering

Scattering of the fundamental harmonic and sum frequency waves is calculated using Mie theory.[40,41] Mie theory requires that the tangential components of the electric and magnetic fields are continuous at the interface. The scattered and the incident field outside the sphere have to add up to match the scattered field inside the sphere:

$$\begin{aligned} E^{\text{sc,i}}_{\theta,\phi} &= E^{\text{sc,o}}_{\theta,\phi} + E^{\text{inc}}_{\theta,\phi}, \\ H^{\text{sc,i}}_{\theta,\phi} &= H^{\text{sc,o}}_{\theta,\phi} + H^{\text{inc}}_{\theta,\phi}. \end{aligned} \tag{1}$$

This set of equations simplifies drastically when all fields are expanded into a set of vector spherical harmonics,

$$\begin{aligned} \begin{Bmatrix} \vec{E} \\ \vec{H} \end{Bmatrix}(\vec{r}) = \begin{Bmatrix} 1 \\ -\frac{ik}{\omega\mu} \end{Bmatrix} \sum_{n=0}^{\infty} \sum_{m=-n}^{n} \begin{Bmatrix} a^{\text{inc}}_{m,n} \\ b^{\text{inc}}_{m,n} \end{Bmatrix} \vec{N}^{(j_{\text{inc}})}_{m,n}(\vec{r}) \\ + \begin{Bmatrix} b^{\text{inc}}_{m,n} \\ a^{\text{inc}}_{m,n} \end{Bmatrix} \vec{M}^{(j_{\text{inc}})}_{m,n}(\vec{r}), \end{aligned} \tag{2}$$

where the vector spherical harmonics $\vec{N}^{(j)}_{mn}(r,\theta,\phi)$ and $\vec{M}^{(j)}_{mn}(r,\theta,\phi)$ are known to satisfy the wave equation. They depend on $\exp(i\phi)$, associated Legendre functions $P^m_n(\cos\theta)$ and spherical Riccati-Bessel functions $\psi^{(j)}_n(kr)$ of kind j. Thus Eq. (1) reduces to a linear equation for the expansion coefficients $a_{m,n}$ and $b_{m,n}$, which makes Mie theory an efficient way to calculate scattering from a sphere,

$$\begin{aligned} & a^{\text{inc}}_{m,n} \begin{pmatrix} \psi^{(j_{\text{inc}})}_n(Rk_{\text{o}}) \\ \frac{1}{Rk_{\text{o}}}\psi^{(j_{\text{inc}})}_n(Rk_{\text{o}})' \end{pmatrix} \\ & = \begin{pmatrix} \psi^{(j_{\text{sc,i}})}_n(Rk_{\text{i}}) & -\psi^{(j_{\text{sc,o}})}_n(Rk_{\text{o}}) \\ \frac{1}{Rk_{\text{i}}}\psi^{(j_{\text{sc,i}})}_n(Rk_{\text{i}})' & -\frac{1}{Rk_{\text{o}}}\psi^{(j_{\text{sc,i}})}_n(Rk_{\text{o}})' \end{pmatrix} \begin{pmatrix} a^{\text{sc,i}}_{m,n} \\ a^{\text{sc,o}}_{m,n} \end{pmatrix}, \\ & b^{\text{inc}}_{m,n} \begin{pmatrix} \frac{1}{Rk_{\text{o}}}\psi^{(j_{\text{inc}})}_n(Rk_{\text{o}}) \\ \psi^{(j_{\text{inc}})}_n(Rk_{\text{o}})' \end{pmatrix} \\ & = \begin{pmatrix} \frac{1}{Rk_{\text{i}}}\psi^{(j_{\text{sc,i}})}_n(Rk_{\text{i}}) & -\frac{1}{Rk_{\text{o}}}\xi^{(j_{\text{sc,o}})}_n(Rk_{\text{o}}) \\ \psi^{(j_{\text{sc,i}})}_n(Rk_{\text{i}})' & -\psi^{(j_{\text{sc,o}})}_n(Rk_{\text{o}})' \end{pmatrix} \begin{pmatrix} b^{\text{sc,i}}_{m,n} \\ b^{\text{sc,o}}_{m,n} \end{pmatrix}. \end{aligned} \tag{3}$$

The above formulation of the matrix becomes numerically unstable for either larger spheres or spheres of high refractive index or spheres consisting of an absorbing material. The equations have to be reformulated to overcome this problem.[42–45] Additionally, the Mie method can be expanded to core-shell particles: Instead of applying the continuity condition to only one interface it is applied to every interface between the core of the particle, its various shells, and the surrounding,[46] resulting again in a linear equation for the expansion coefficients inside and outside the sphere.

In classical Mie theory, the incident electric and magnetic fields are assumed to be plane waves. The expansion

coefficients for a plane wave, polarized parallel to the X axis [$\vec{E}_{\mathrm{FH},1} = \vec{E}_1 \exp(ik_1 r\cos\theta)$], are[47]

$$a_{m,n} = -i^{n+1}\frac{2n+1}{2n(n+1)}(\delta_{m,1}+\delta_{m,-1}), \tag{4}$$

$$b_{m,n} = -i^{n+1}\frac{2n+1}{2n(n+1)}(\delta_{m,1}-\delta_{m,-1}). \tag{5}$$

However, arbitrary incident fields can be expanded into vector spherical harmonics, which leads to a generalized Mie theory[48] with respective expansion coefficients $a^{\mathrm{inc}}_{m,n}$ and $b^{\mathrm{inc}}_{m,n}$ as input parameters in Eq. (3). It is therefore possible to calculate the resulting field of a dipole placed anywhere near a spherical particle.

C. Nonlinear polarization

The scattered fundamental harmonic fields give rise to a nonlinear polarization $\vec{P}^{(2)}$, that describes the surface density of oscillating electric dipoles (SI unit Cm/m^2). In the case of a pure $\chi^{(2)}$ effect, $\vec{P}^{(2)}$ is given by

$$P^{(2)}_i = \sum_{j=1}^{3}\sum_{k=1}^{3}\chi^{(2)}_{ijk}E^{\mathrm{FH},1}_j E^{\mathrm{FH},2}_k. \tag{6}$$

Additionally, $\chi^{(3)}$ effects can lead to second harmonic generation when a static electric field is present, e.g., a radially polarized electric field Φ from the surface charge of the sphere:[49]

$$P^{(2)}_i = \sum_{j=1}^{3}\sum_{k=1}^{3}\chi^{(3)}_{ijk3}E^{\mathrm{FH},1}_j E^{\mathrm{FH},2}_k\Phi_3. \tag{7}$$

This nonlinear polarization $\vec{P}^{(2)}$ gives rise to an electromagnetic sum frequency field:

$$\vec{E}^{(2)}(\vec{r}) \propto \int d\vec{r}\,'\,\vec{P}^{(2)}(\vec{r}\,'). \tag{8}$$

The nonlinear surface susceptibility $\chi^{(2)}_{ijk}$ is a property of the surface material (gold, polystyrene) or of molecules that are adsorbed to the surface or oriented close to the surface due to electric fields.

In the case of molecules, $\chi^{(2)}_{ijk}$ (SI unit m^2/V) can be calculated from the molecular hyperpolarizability β_{ijk} (SI unit C^3 m^3/J^2), the molecular orientation with respect to the macroscopic coordinate frame and additional fields due to the presence of surrounding molecules,[50]

$$\begin{aligned}\chi^{(2)}_{ijk} = &\sum_{l,m,n=1}^{3} f_{il}(\omega_1+\omega_2)f_{jm}(\omega_1)f_{kn}(\omega_2)\\ &\times\int d\alpha\int d\beta\int d\gamma\ \ \rho(\alpha,\beta,\gamma)\\ &\times\sum_{o,p,q=1}^{3} M_{lo}(\alpha,\beta,\gamma)M_{mp}(\alpha,\beta,\gamma)M_{nq}(\alpha,\beta,\gamma)\beta_{opq},\end{aligned} \tag{9}$$

where $\rho(\alpha,\beta,\gamma)$ denotes the orientational density distribution of the molecules. The rotation from the molecular coordinate frame with respect to the local coordinate frame of the surface

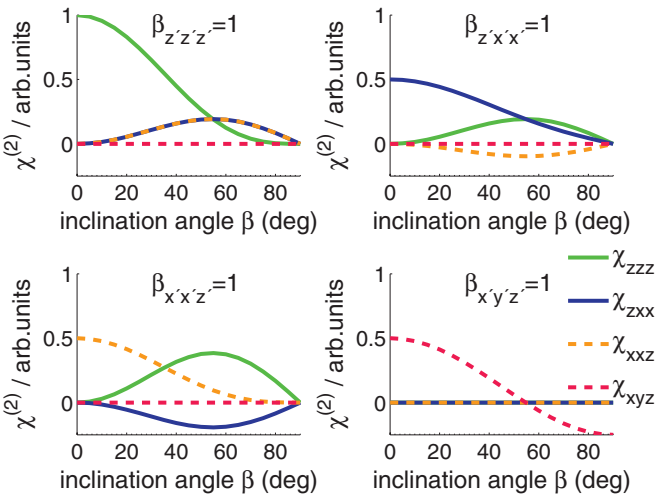

FIG. 2. (Color online) $\chi^{(2)}_{ijk}$ calculated from a single $\beta_{i'j'k'}$ component for an increasing inclination angle β of the molecular z' axis with respect to the surface normal (z axis). In all plots a uniform distribution of the molecule axis is assumed and respective coefficients of the molecular susceptibility are kept constant.

of the sphere is given by the Euler angles α,β,γ and the respective rotation matrix $M(\alpha,\beta,\gamma)$. At optical frequencies and isotropy of the interface the local field correction factors can be found from the Lorentz local field $f_{ij}(\omega) = \frac{\epsilon(\omega)+2}{3}$.

If there is no global order we can assume that the molecules are rotated arbitrarily around the surface normal ($\gamma = [0,2\pi]$) so that from 27/18 independent components of β in the case of SFG/SHG, only 7/4 independent components of $\chi^{(2)}$ remain. If the molecules are also rotated arbitrarily around their molecular axis ($\alpha = [0,2\pi]$) and are all inclined by the same fixed angle β, Eq. (9) can be simplified. For example, $\chi^{(2)}_{zzz}$ in the case of SHG is given by

$$\begin{aligned}\chi^{(2)}_{zzz} \propto &\sin\beta\sin 2\beta\frac{\beta_{xxz}+\beta_{yyz}}{2}\\ &+\sin^2\beta\cos\beta\frac{\beta_{zxx}+\beta_{zyy}}{2}+\beta_{zzz}\cos^3\beta.\end{aligned} \tag{10}$$

From Eq. (9) the susceptibilities of a given angular distribution and hyperpolarizability can be calculated (see Fig. 2).

The chiral component β_{xyz} does not mix with the other three independent components. When the molecular β_{ijk} is known and the relevant $\chi^{(2)}_{ijk}$ components are extracted from the measurement, the surface coverage and the average inclination angle β can be calculated.

D. Nonlinear dipoles

The action of the nonlinear surface polarization $\vec{P}^{(2)}$ is modeled directly by placing elementary electric dipoles at positions $\vec{r}_i$ at the surface of the sphere, where the density of dipoles is chosen sufficiently high to achieve convergence of the far field but calculation time is kept short. We used typically several hundred of dipoles, depending on the radius of the sphere.

At each position the polarization $\vec{P}^{(2)}$ is calculated in a coordinate frame with its z axis normal to the surface of the sphere and the x axis pointing to the pole (see Fig. 1). P_x, P_y,

and P_z indicate the intensity of dipoles with axis parallel to the x, y, and z axis, respectively.

To calculate scattering of these elementary dipoles at the sphere the dipole fields are expressed by vector spherical harmonics. Electric dipoles located at the origin are given by

$$\vec{E}_{\mathrm{Dipole},z} = \vec{N}^{(3)}_{0,1}, \tag{11}$$

$$\vec{E}_{\mathrm{Dipole},x/y} = \vec{N}^{(3)}_{1,1} \pm 2\vec{N}^{(3)}_{-1,1}. \tag{12}$$

Contrary to a plane wave, bessel functions of third kind (Hankel functions) are needed, denoted by $j = 3$.

The dipole is then shifted to the surface of the sphere using an addition theorem for translation.[51] Whereas only one order of expansion ($n = 1, m = \pm 1, 0$) is needed for a dipole placed at the origin, the expansion of a dipole that is shifted about a distance d converges pointwise in space. Only a small number of orders is needed for convergences close to the origin or for a point with $|\vec{r}| \gg d$. As $|\vec{r}| \to d$, the number of orders needed for convergence goes to infinity. In our simulation, the number of orders is chosen so that at the distance of detection the scattered fields converge. Depending on the radius of the sphere and the refractive index, typically 5 to 20 orders are needed.

In a second step, the expansion coefficients $a^{(\mathrm{Dipole,\ sc},\ z/x/y)}_{m,n}$ and $b^{(\mathrm{Dipole,\ sc},\ z/x/y)}_{m,n}$ for the scattered dipole fields are calculated using linear Mie theory with expansion coefficients for the translated dipoles $a^{(\mathrm{Dipole,\ tr},\ z/x/y)}_{m,n}$ and $b^{(\mathrm{Dipole,\ tr},\ z/x/y)}_{m,n}$ as expansion coefficients for the incident field. The same linear boundary conditions (continuity of the tangential fields) are used as for scattering of a plane wave. Back action of the second harmonic fields onto the fundamental harmonic fields is not considered. The latter assumption is valid as long as the second harmonic fields remain weak so that down conversion can be neglected. This is extremely well justified for all realistic situations, where nanoparticles are involved. Due to this approximation the system becomes effectively linear and Mie theory can be applied.

The scattered fields have to be calculated only for one dipole position, as the expansion coefficients of the scattered fields can be rotated to the positions of other dipoles using a rotation addition theorem.[52] The expansion coefficients of all fields emitted by dipoles with magnitudes $P^{(2)}_i$ and scattered at the sphere, are added to give the expansion coefficients of the total second harmonic field.

To summarize, the simulation steps are given for second harmonic generation. a is always meant to represent both expansion coefficients $a_{m,n}$ and $b_{m,n}$.

(1) As a preparation the linear scattering of the plane wave and the three dipoles ($x/y/z$) is calculated:

(a) Scattering of a plane wave:

$a_{\mathrm{FH}} = \texttt{planeWave}(\lambda_{\mathrm{FH}})$,

$a_{\mathrm{FH,sc}} = \texttt{MieScattering}(a_{\mathrm{FH}})$.

(b) Scattering of the three dipoles parallel to x, y, and z:

$a_{\mathrm{D},\substack{x\\y\\z}} = \texttt{dipole}(\frac{1}{2}\lambda_{\mathrm{FH}}, \substack{x\\y\\z})$,

$a_{\mathrm{D,tr},\substack{x\\y\\z}} = \texttt{translation}(a_{\mathrm{D},\substack{x\\y\\z}}, |\vec{r}_i|)$,

$a_{\mathrm{D,sc},\substack{x\\y\\z}} = \texttt{MieScattering}(a_{\mathrm{D,tr},\substack{x\\y\\z}})$.

(2) Discrete positions $\vec{r}_i$ at the surface of the sphere, where $P^{(2)} \neq 0$, are chosen. For every $\vec{r}_i$, the scattered dipoles are rotated to $\vec{r}_i$:

$a_{\mathrm{D,sc},\substack{x\\y\\z},i} = \texttt{rotation}(a_{\mathrm{D,sc},\substack{x\\y\\z}}, \vec{r}_i)$.

(3) The actual fundamental harmonic field $\vec{E}(\vec{r}_i)$ at each position $\vec{r}_i$ is calculated from $a_{\mathrm{FH,sc}}$ and used to determine the polarization $\vec{P}^{(2)}$:

$P^{x}_{\substack{y\\z}}{}^{(2)}(\vec{r}_i) = \sum_{j,k} \chi^{x}_{\substack{y\\z}}{}^{(2),j,k} E_j(\vec{r}_i) E_k(\vec{r}_i)$.

(4) The expansion coefficients for the second harmonic field is calculated as a sum over all $\vec{r}_i$:

$a_{\mathrm{SH}} = \sum_i [a_{\mathrm{D,sc},x,i} \cdot P^{(2)}_x(\vec{r}_i) + a_{\mathrm{D,sc},y,i} \cdot P^{(2)}_y(\vec{r}_i) + a_{\mathrm{D,sc},z,i} \cdot P^{(2)}_z(\vec{r}_i)]$.

(5) Finally, the SH intensities are calculated from a_{SH}:

$E_{\mathrm{SH}} = \sum_{m,n} a^{\mathrm{SH}}_{m,n} \vec{N}^{(3)}_{m,n} + b^{\mathrm{SH}}_{m,n} \vec{M}^{(3)}_{m,n}$.

In contrast to other nonlinear Mie models,[28–31,33] the nonlinear polarization is not restricted to a homogeneous layer at the surface of the sphere. Thus our method allows for the simulation of complex systems with several molecular layers, with inhomogeneous coverage of the sphere or with domains of oriented molecules.

III. RESULTS

A. Angular profile of different χ components

The angular distribution of the emitted SH field generally shows distinct peaks for specific polarization combinations (see Fig. 3). We have to keep in mind that the polarization of the exiting as well as that of the generated field can be either parallel or perpendicular to the scattering plane (X-Z plane in Fig. 1) in the experiment. The polarization of the respective FH and SH fields is denoted by indices s or p. For sum frequency scattering, the notation $I_{\mathrm{SF,\ FH1,\ FH2}}$ is used, for second harmonic scattering the polarization combinations are named $I_{\mathrm{FH,SH}}$. SH scattering is symmetric with respect to the propagation direction of the fundamental harmonic. For nonchiral susceptibilities ($\chi^{(2)}_{zzz}$, $\chi^{(2)}_{zxx}$, $\chi^{(2)}_{xxz}$, and $\chi^{(2)}_{xzx}$) all intensities with an even number of s-polarized waves [I_{ppp} ($= I_{\mathrm{pp}}$), I_{pss} ($= I_{\mathrm{sp}}$), I_{sps}, and I_{ssp}] remain.[32,37] The case of chiral susceptibilities ($\chi^{(2)}_{xyz}$, $\chi^{(2)}_{xzy}$, $\chi^{(2)}_{zxy}$) was not considered. Here exactly the complementary intensities I_{pps}, I_{psp}, I_{spp}, and I_{sss} are nonzero. In contrast to the RGD theory,[37] I_{sss} is nonzero when a refractive index contrast is present. Note that chiral β components only contribute to chiral $\chi^{(2)}$ components and vice versa.

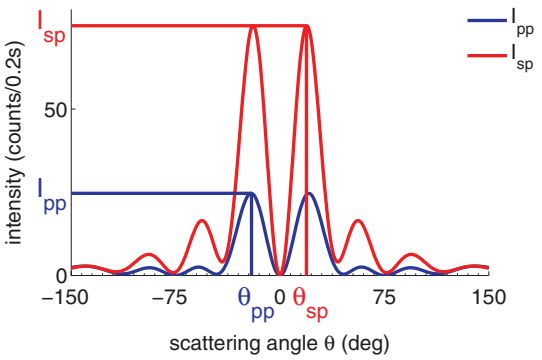

FIG. 3. (Color online) Simulated angular scattering pattern (535-nm diameter polystyrene sphere with $\chi^{(2)}_{zxx}$ as only nonzero component). The positions of the first maximum in sp and pp polarization (θ_{sp}, θ_{pp}) as well as the maximum intensities in I_{sp} and I_{pp} are indicated. These values are used to scan for matching $\chi^{(2)}$ components (compare Fig. 4).

We have already shown that the angular position of the first maximum in both polarizations (θ_{pp}, θ_{sp}) as well as the intensity ratio I_{pp}/I_{sp} of these maxima are good experimental quantities that can be used to determine the relative magnitude of the $\chi^{(2)}_{ijk}$ components.[53,54] Here we aim for a systematic evaluation of the effect of $\chi^{(2)}_{ijk}$ on θ_{pp}, θ_{sp}, and I_{pp}/I_{sp}.

As chiral β components are rare, we restrict our evaluation to the three independent components $\chi^{(2)}_{zzz}$, $\chi^{(2)}_{zxx}$, and $\chi^{(2)}_{xxz}$ for SH scattering. The absolute magnitude of $\chi^{(2)}_{ijk}$ only affects the absolute intensity of the SH light, but not its angular shape. θ_{pp}, θ_{sp}, and I_{pp}/I_{sp} only depend on the relative magnitude of $\chi^{(2)}_{zzz}$, $\chi^{(2)}_{zxx}$, and $\chi^{(2)}_{xxz}$, which can be negative or positive, displaying the arbitrarity when choosing the direction of a positive x, y, or z axis. As $(\chi^{(2)}_{zzz}, \chi^{(2)}_{zxx}, \chi^{(2)}_{xxz}) = (+1, -1, -1)$ is equivalent to $(\chi^{(2)}_{zzz}, \chi^{(2)}_{zxx}, \chi^{(2)}_{xxz}) = (-1, +1, +1)$ we consider the four cases, where either all three independent $\chi^{(2)}$ components are positive or only one of them is negative.

The dependence of a function on the relative magnitude of three variables $f(a,b,c)$ can be displayed, similar to the color triangle of the Commission Internationale de l'Éclairage (CIE)[55] or a ternary phase diagram, by converting (a,b,c) to a two-dimensional coordinate $(x,y) = (\frac{a+0.5b}{a+b+c}, \frac{b}{a+b+c})$ $(a,b,c > 0)$. This results in a triangle with corners $(x,y) = (0,0)$ corresponding to $(a,b,c) = A(0,0,1)$, $(x,y) = (1,0)$ corresponding to $(a,b,c) = A(1,0,0)$ and $(x,y) = (0.5,1)$ corresponding to $(a,b,c) = A(0,1,0)$, where A is an arbitrary factor. To account for negative a, b, or c, triangles calculated using the absolute values for a, b, and c can be mirrored at the respective edge of the triangle. The result is a large triangle, consisting of four small triangles.

In that way, it is possible to display θ_{pp}, θ_{sp}, and I_{pp}/I_{sp} as a function of all possible combinations of $(\chi^{(2)}_{zzz}, \chi^{(2)}_{zxx}, \chi^{(2)}_{xxz})$ in three single color map plots (see Fig. 4). We find that the intensity ratio varies at least by five orders of magnitude (10^{-2} to 10^{3} for a $R = 100$-nm polystyrene sphere in water)

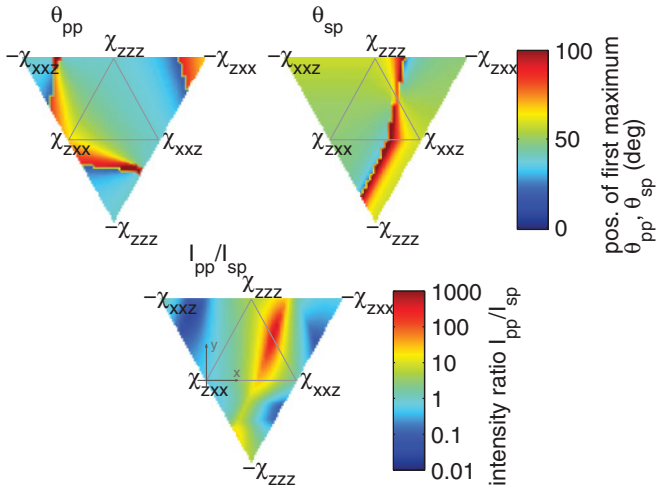

FIG. 4. (Color online) Position of the first maximum in *sp* and *pp* polarization (θ_{pp},θ_{sp}) and ratio of peak intensity of the first maxima (I_{pp}/I_{sp}) for various values of $(\chi^{(2)}_{zzz}, \chi^{(2)}_{zxx}, \chi^{(2)}_{xxz})$ and a polystyrene sphere of 100 nm radius in water. At the corners of the inner and the three outer triangles, only one component of $\chi^{(2)}$ is nonzero. The respective component is indicated in the graph.

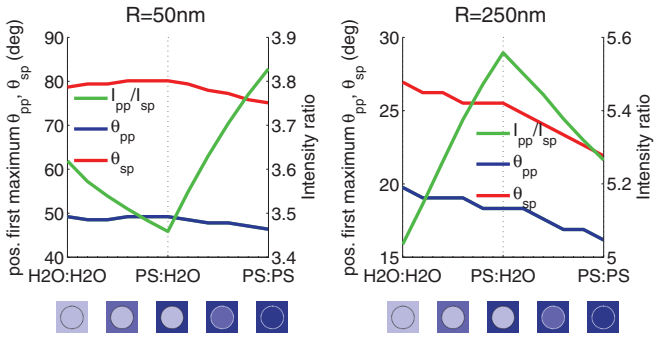

FIG. 5. (Color online) Effect of refractive index contrast between sphere and solvent on the SH light and for $\chi^{(2)}_{zzz}$ being the only nonvanishing coefficient. The material of the sphere and surrounding are indicated on the x axis, ranging from a water sphere emersed in water (H2O:H2O, RGD limit), via a polystyrene sphere in water (PS:H2O), to a polystyrene sphere immersed in polystyrene (PS:PS, RGD limit).

and is therefore an especially significant parameter when comparing experimental results to the simulation in order to find a matching $\chi^{(2)}_{ijk}$.

B. Comparison with Rayleigh-Gans-Debye theory

To study the effect of a refractive index contrast and to check the numerical stability of our code, we compare it to the analytical RGD theory.[11] For vanishing refractive index contrast and dispersion, the results of our model and the analytical solution of the RGD theory[11] coincide for all nonchiral components of $\chi^{(2)}$, with $\beta_{ccc} = \chi^{(2)}_{zzz}$, $\beta_{aac} = \beta_{aca} = \chi^{(2)}_{xxz}$, $\beta_{caa} = \chi^{(2)}_{zxx}$ $(\phi = 0)$.

Figure 5 shows the effect of an increasing refractive index constrast, for which the system starts to deviate from the RGD limit. Starting from the RGD limit of a water sphere in water ($n_{surr.} = n_{sphere} = 1.3$), the refractive index of the sphere is increased to $n_{sphere} = 1.6$ (polystyrene sphere in water). Then the refractive index of the surrounding is also increased to $n_{surr.} = 1.6$ (polystyrene sphere in polystyrene, RGD limit). As already shown by Jen *et al.*[56] even in RGD theory, the refractive index has a significant impact on the scattering angles of secondary maxima (PS:PS vs H2O:H2O limits in Fig. 5). But even for small spheres ($\frac{2\pi R}{\lambda}|\frac{n_1}{n_2} - 1| = 0.074$ for the $R = 50$-nm sphere), the intensity ratio depends noticeably on the changing refractive index ratio, an effect, which is not accounted for in RGD theory.

Figure 6 shows a systematic comparison of our results for a polystyrene sphere in water compared to the RGD theory with the refractive index of water for all possible combinations of $(\chi^{(2)}_{zzz}, \chi^{(2)}_{zxx}, \chi^{(2)}_{xxz})$. We find that for pure $\chi^{(2)}_{zzz}$, $\chi^{(2)}_{zxx}$, or $\chi^{(2)}_{xxz}$ (corners of the inner triangle), the difference $\frac{|X_{RGD} - X_{Mie}|}{(X_{RGD} + X_{Mie})/2}$ is negligible. However, for certain values for $\chi^{(2)}_{ijk}$, the difference between both methods is as large as $\frac{|X_{RGD} - X_{Mie}|}{(X_{RGD} + X_{Mie})/2} = 200\%$. The angular scattering profile for two $\chi^{(2)}_{ijk}$ combinations are given in Fig. 7. This is particularly surprising because this comparison was performed for polystyrene spheres suspended in water where the index contrast is moderate. In that case one would have expected RGD theory to be completely valid. For

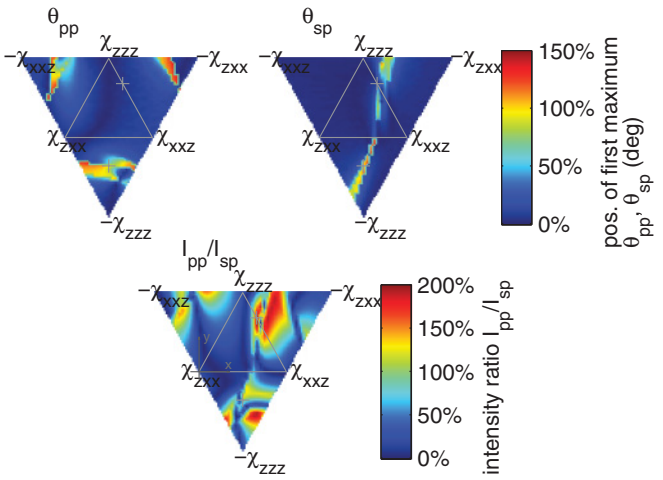

FIG. 6. (Color online) Difference $\frac{|X_{\mathrm{RGD}}-X_{\mathrm{Mie}}|}{(X_{\mathrm{RGD}}+X_{\mathrm{Mie}})/2}$ between the results from RGD (X_{RGD}) and Mie (X_{Mie}) theory for a $R = 100$-nm polystyrene sphere in water. Coordinates $(x, y) = (0, -0.36)$ and $(0.16, 0.68)$ are indicated by a +; the corresponding angular scattering profiles are shown in Fig. 7.

higher values of the index contrast as they occur for metallic particles the differences between the RGD and the Mie theory become even more pronounced.

C. Size dependence

For increasing sphere radius the scattered field transforms from a more uniform angular distribution into a radiation pattern with pronounced lobes pointing in the forward direction as already shown by Jen *et al.*[57] In Fig. 8 the simulated signals from a polystyrene and gold sphere, both suspended in water, are shown.

A strong resonance with signal enhancement by one order of magnitude is observed for the metallic sphere for $R = 100$ nm and for $\chi^{(2)}_{zzz}$ being the only nonvanishing coefficient (as only I_{pp} is increased, the intensity ratio displays this resonance). Mie resonances for metallic particle have already been observed by Östling *et al.*[28]

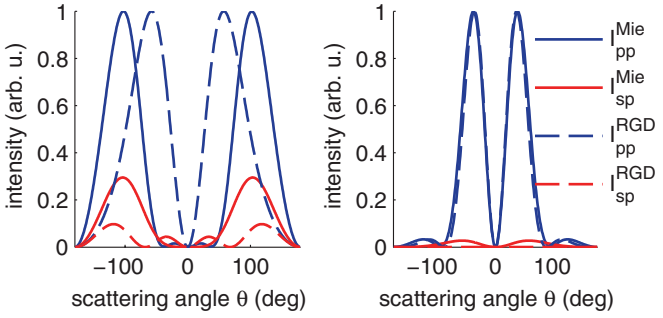

FIG. 7. (Color online) Angular scattering profile for a $R = 100$-nm polystyrene sphere in water, calculated using Mie theory (solid lines) and RGD theory (dashed lines, using the refractive index of water). Left: $\chi^{(2)}_{zzz}/\chi^{(2)}_{zxx} = -1.13$, $\chi^{(2)}_{xxz}/\chi^{(2)}_{zxx} = 1$. Right: $\chi^{(2)}_{zzz}/\chi^{(2)}_{xxz} = 2.13$, $\chi^{(2)}_{zxx} = 0$. The corresponding coordinates in Fig. 6 are $(x, y) = (0, -0.36)$ and $(0.16, 0.68)$.

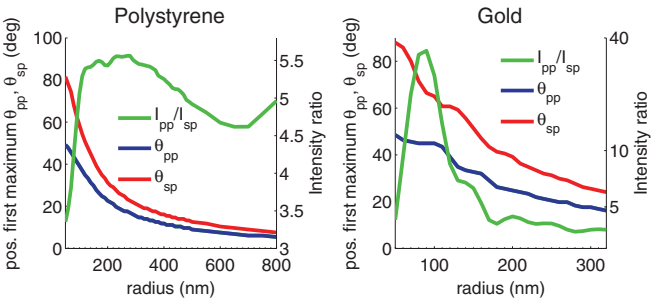

FIG. 8. (Color online) SH signal for varying radius of a polystyrene or gold sphere in water and for $\chi^{(2)}_{zzz}$ being the only nonvanishing coefficient.

D. Dipoles protruding the surface of the sphere

Larger, chainlike molecules cannot be assumed to be situated just on the surface of a nanosphere. We model such a situation by placing several dipoles with different distance to the surface of the sphere. This approach has been used to study the shell layer of spherical polyelectrolyte brushes, particles consisting of a polystyrene core and a shell of highly charged linear polyelectrolyte chains.[54]

Figure 9 (left) displays the dependence of θ_{pp}, θ_{sp}, and $I_{\mathrm{pp}}/I_{\mathrm{sp}}$ on the distance (ranging from 0 to 200 nm) of a thin monolayer of dipoles from the surface of the sphere. The right-hand side of Fig. 9 shows the dependence of θ_{pp}, θ_{sp}, and $I_{\mathrm{pp}}/I_{\mathrm{sp}}$ on the thickness (ranging from 0 to 200 nm) of a layer of dipoles placed with a distance of 100 nm to the surface of the sphere, thus being the coherent sum of various thin monolayers of the left-hand side.

With increasing distance, the scattering becomes more pronounced in the forward direction, similar to the nonlinear scattering from a sphere of larger radius. But the intensity ratio behaves differently so that a system where the polarization is not concentrated at the surface of the sphere can, at least in theory, be distinguished from the case where just the radius of the sphere is increased (compare to Fig. 8). The length of a

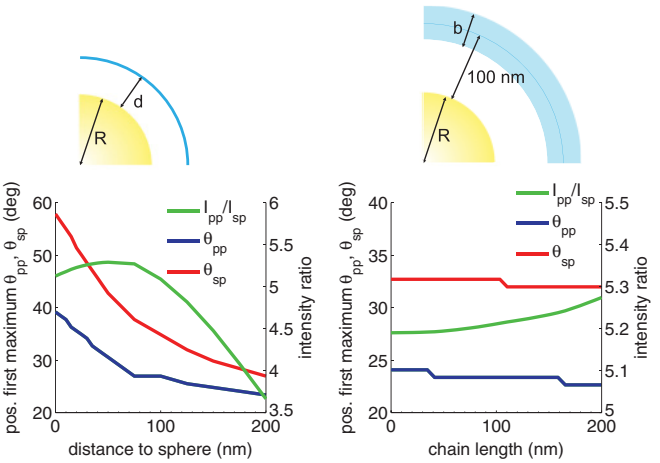

FIG. 9. (Color online) SH signal from a $R = 100$-nm polystyrene sphere in water with $\chi^{(2)}_{zzz}$. Left: The distance d between the dipoles and the surface of the sphere was varied. Right: The length b of a chain of ten equally spaced dipoles with center-of-mass distance $d = 100$ nm was varied.

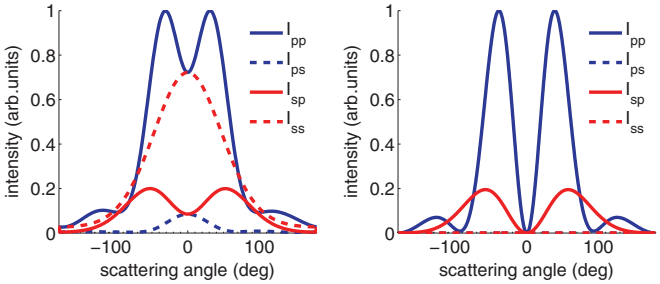

FIG. 10. (Color online) Scattering profile of a $R = 100$-nm sphere that is only half covered with molecules (left) in comparison to a fully covered sphere (right).

chain of dipoles with center-of-mass distance $d = 100$ nm to the surface of the sphere on the other hand hardly affects the position of the first maxima and the intensity ratio. However, it has an impact on the scattering profile.[54]

E. Partly covered sphere

A unique feature of the presented model is its ability to simulate systems with an inhomogeneous distribution of $\chi^{(2)}$-active molecules around the sphere, a model applicable to certain seeded growth processes. Of course we have to assume that the inhomogeneous coverage does not affect linear scattering processes. In Fig. 10 we show the SH scattering profile of a polystyrene sphere in water that is only half covered with molecules.

One hemisphere of a polystyrene sphere in water ($n \approx 1.3/1.6$) with $R = 100$ nm radius was covered with nonlinear dipoles (pure $\chi^{(2)}_{zzz}$) and the second harmonic fields were calculated. This process was repeated for various arbitrary orientations of the hemisphere with respect to the propagation direction of the fundamental harmonic laser (z axis) and all intensities are averaged incoherently.

Whereas for completely covered spheres, the intensities I_{ps} and I_{ss} are zero for all scattering angles, due to broken symmetry in the case of a partly covered sphere, these intensities do not vanish anymore and the minima no longer drop to zero intensity.

F. Comparison with experimental results for malachite green adsorbed to polystyrene spheres

We have already shown, that our model is able to determine the ratio of the local surface susceptibility elements.[53,54] Here we use the nonlinear Mie model to investigate the surface susceptibility of malachite green molecules adsorbed to polystyrene spheres. Malachite green on a nonmetallic surface has already been studied by others,[33,56,58,59] but their findings are inconsistent.

For a planar fused silica-air interface with adsorbed malachite green molecules, Kikteva[58] found a dominant $\chi^{(2)}_{zxx}$ component at $\lambda_{FH} = 800$ nm, which agrees with the electronic structure of malachite green, where the $S_2 \leftarrow S_0$ transition is resonant at 410 nm.

Yang *et al.*[59] performed the first angle-resolved scattering experiment for polystyrene spheres with diameters 980, 700, and 510 nm and adsorbed malachite green. The measured

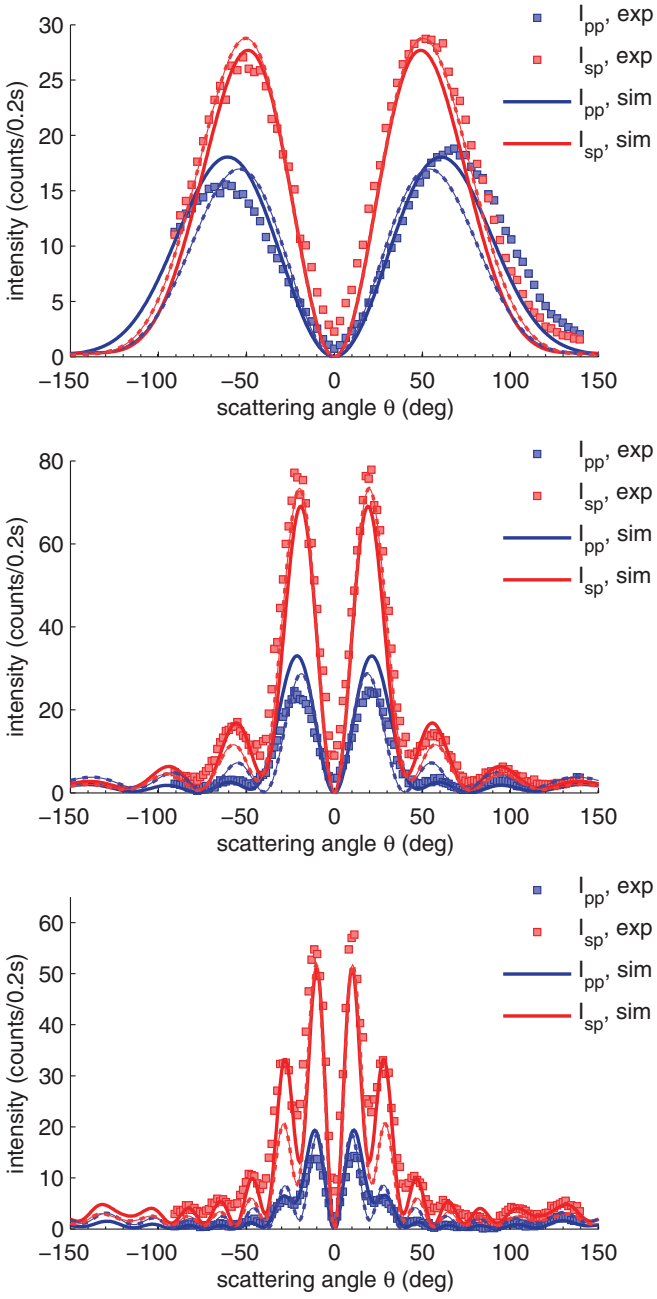

FIG. 11. (Color online) Corrected SH scattering profiles in *pp* and *sp* polarization configuration from 200-nm (top), 535-nm (middle), and 989-nm (bottom) polystyrene particles with malachite green. The simulated scattering profiles (solid lines) for $\chi^{(2)}_{zzz}/\chi^{(2)}_{zxx} = 0.14$ and $\chi^{(2)}_{xxz}/\chi^{(2)}_{zxx} = -0.027$ are scaled to fit the experimental data. Dashed lines show simulations for $\chi^{(2)}_{zzz}/\chi^{(2)}_{zxx} = 0.43$ and $\chi^{(2)}_{xxz}/\chi^{(2)}_{zxx} = -0.23$, according to the results of Gonella and Dai (Ref. 33).

$I_{pp}(\theta)$ agreed well with their RGD simulations using a pure $\chi^{(2)}_{zzz}$ component. However, they did not consider the ratio I_{pp}/I_{sp} or $I_{sp}(\theta)$ in their analysis.

Jen *et al.*[56] used polystyrene particles with diameters ranging from 56 to 1053 nm, $\lambda = 840$ nm, and a RGD model to fit I_{pp} and I_{sp}. Using the refractive index of water, they found $\chi^{(2)}_{zxx}$ as dominating component for small particles (diameter 202, 88, and 56 nm), but argue that due to the small particle

size, they could not determine the exact ratio of the $\chi^{(2)}$ components. For particles of 1053 nm diameter, however, the best fit was achieved using a dominant $\chi^{(2)}_{zzz}$ ($\chi^{(2)}_{zzz}/\chi^{(2)}_{zxx} = -2.2$, $\chi^{(2)}_{xxz}/\chi^{(2)}_{zxx} = -0.5$) and an refractive index matching that of the particle. Recently they also analyzed the experimental data using a nonlinear Mie model.[33] For all particle sizes they found $\chi^{(2)}_{\perp\perp\perp}/\chi^{(2)}_{\perp\parallel\parallel} = 0.43$ and $\chi^{(2)}_{\parallel\perp\parallel}/\chi^{(2)}_{\perp\parallel\parallel} = -0.23$, however, their experimental data end between $\theta = 85^\circ$ and $\theta = 120^\circ$ and are displayed as an angular plot, which makes it difficult to compare the experimental and the simulated SH profiles in detail.

Here, we present measurements of the second harmonic light scattering from polystyrene particles (Polysciences, plain surface functionalization) with diameter 200, 535, and 989 nm with adsorbed malachite green at *p*H 4 and 800-nm fundamental harmonic wavelength. The experimental setup and the correction procedure for hyper-Rayleigh scattering from the background solution are described in detail in Ref. 53. The angular scattering profiles are shown in Fig. 11. We used the position of the first maximum in *pp* and *sp* polarization (θ_{pp}, θ_{sp}) and the ratio of the peak intensities I_{pp}/I_{sp} to limit the range of possible ratios $\chi^{(2)}_{zzz}/\chi^{(2)}_{zxx}$ and $\chi^{(2)}_{xxz}/\chi^{(2)}_{zxx}$ for positive and negative $\chi^{(2)}$ components. Even though the position of the maximum for small spheres does not vary much for different $\chi^{(2)}$ components, as already described by Jen *et al.*,[56] the intensity ratio $I_{pp}/I_{sp} = 0.6$ for $R = 100$ nm limits the range of possible $\chi^{(2)}$ components and does not allow for a dominating $\chi^{(2)}_{zzz}$ component, where $I_{pp}/I_{sp} > 1$ (compare Fig. 4). We limited the range of $\chi^{(2)}$ components that fulfill I_{pp}/I_{sp}, θ_{pp}, and θ_{sp} by checking the position and intensities of additional maxima at higher scattering angles. In agreement with Kikteva *et al.*,[58] we found a susceptibility with dominating $\chi^{(2)}_{zxx}$. Independent of the sphere diameter, the ratio of the susceptibility components, used to fit the experimental data, are $\chi^{(2)}_{zzz}/\chi^{(2)}_{zxx} = 0.14$ and $\chi^{(2)}_{xxz}/\chi^{(2)}_{zxx} = -0.027$. The susceptibility $\chi^{(2)}_{zzz}/\chi^{(2)}_{zxx} = 0.43$ and $\chi^{(2)}_{xxz}/\chi^{(2)}_{zxx} = -0.23$ as found by Gonella and Dai[33] for $\lambda = 840$ nm did not fit to the position and intensity of the secondary maxima observed in our experiment. Apart from the different wavelength, also the surface properties of the particles used could have been different, thus resulting in a different $\chi^{(2)}$.

IV. CONCLUSION

In conclusion, we have developed a model for second harmonic and sum frequency scattering from centrosymmetric spherical particles of arbitrary size and material composition. By modeling the nonlinear polarization directly as an ensemble of individual dipoles the theory offers great flexibility that can be used to simulate the SH signal from large molecules adsorbed to spheres or from particles generated in seeded-growth processes resulting in inhomogeneous covered spheres.

We have compared the full Mie solution to the widely used Rayleigh-Gans-Debye approximation for the case of a polystyrene sphere of 100 nm radius in water and found significant deviations especially for the ratio of the signal intensities in different polarization combinations, even for systems with moderate index contrast. Experimental scattering profiles for polystyrene spheres with adsorbed malachite green could be fitted using the nonlinear Mie model. We were able to determine the surface susceptibility of the system to be $\chi^{(2)}_{zzz}/\chi^{(2)}_{zxx} = 0.14$ and $\chi^{(2)}_{xxz}/\chi^{(2)}_{zxx} = -0.027$, independent of sphere diameter.

ACKNOWLEDGMENTS

The authors gratefully acknowledge funding of the Erlangen Graduate School in Advanced Optical Technologies (SAOT) and the Cluster of Excellence Engineering of Advanced Materials (EAM) by the German Research Foundation (DFG) in the framework of the German excellence initiative.

*Also at EAM Cluster of Excellence Engineering of Advanced Materials and Erlangen Graduate School in Advanced Optical Technologies (SAOT), University of Erlangen-Nuremberg, Erlangen, Germany.

†sarina.wunderlich@mpl.mpg.de

[1] T. F. Heinz, C. K. Chen, D. Ricard, and Y. R. Shen, Phys. Rev. Lett. **48**, 478 (1982).

[2] T. F. Heinz, H. W. K. Tom, and Y. R. Shen, Phys. Rev. A **28**, 1883 (1983).

[3] H. Wang, E. C. Y. Yan, E. Borguet, and K. B. Eisenthal, Chem. Phys. Lett. **259**, 15 (1996).

[4] J. Martorell, R. Vilaseca, and R. Corbalán, in *QELS*, Vol. 16 (OSA, Washington, DC, 1995), p. 32.

[5] E. C. Y. Yan, Y. Liu, and K. B. Eisenthal, J. Phys. Chem. B **102**, 6331 (1998).

[6] H. Wang, T. Troxler, A.-G. Yeh, and H.-L. Dai, Langmuir **16**, 2475 (2000).

[7] S. Roke, O. Berg, J. Buitenhuis, A. van Blaaderen, and M. Bonn, Proc. Natl. Acad. Sci. USA **103**, 13310 (2006).

[8] M. Subir, J. Liu, and K. B. Eisenthal, J. Phys. Chem. C **112**, 15809 (2008).

[9] H. B. de Aguiar, A. G. F. de Beer, M. L. Strader, and S. Roke, J. Am. Chem. Soc. **132**, 2122 (2010).

[10] H. B. de Aguiar, M. L. Strader, A. G. F. de Beer, and S. Roke, J. Phys. Chem. B **115**, 2970 (2011).

[11] A. G. F. de Beer and S. Roke, J. Chem. Phys. **132**, 234702 (2010).

[12] W. Gan, B. Xu, and H.-L. Dai, Angew. Chem. Int. Ed. **50**, 6622 (2011).

[13] R. Vácha, S. W. Rick, P. Jungwirth, A. G. F. de Beer, H. B. de Aguiar, J.-S. Samson, and S. Roke, J. Am. Chem. Soc. **133**, 10204 (2011).

[14] L. H. Haber, S. J. J. Kwok, M. Semeraro, and K. B. Eisenthal, Chem. Phys. Lett. **507**, 11 (2011).

[15] A. G. F. de Beer, H. B. de Aguiar, J. F. W. Nijsen, and S. Roke, Phys. Rev. Lett. **102**, 095502 (2009).

[16] J. I. Dadap, H. B. de Aguiar, and S. Roke, J. Chem. Phys. **130**, 214710 (2009).

[17]J. Griffin, A. K. Singh, D. Senapati, E. Lee, K. Gaylor, J. Jones-Boone, and P. C. Ray, Small **5**, 839 (2009).
[18]C.-L. Hsieh, R. Grange, Y. Pu, and D. Psaltis, Biomaterials **31**, 2272 (2010).
[19]J. Jiang, K. B. Eisenthal, and R. Yuste, Biophys. J. **93**, L26 (2007).
[20]Y. Liu, E. C. Y. Yan, and K. B. Eisenthal, Biophys. J. **80**, 1004 (2001).
[21]G. S. Agarwal and S. S. Jha, Solid State Commun. **41**, 499 (1982).
[22]J. I. Dadap, J. Shan, K. B. Eisenthal, and T. F. Heinz, Phys. Rev. Lett. **83**, 4045 (1999).
[23]J. I. Dadap, J. Shan, and T. F. Heinz J. Opt. Soc. Am. B **21**, 1328 (2004).
[24]V. L. Brudny, B. S. Mendoza, and W. L. Mochán, Phys. Rev. B **62**, 11152 (2000).
[25]W. L. Mochán, J. A. Maytorena, B. S. Mendoza, and V. L. Brudny, Phys. Rev. B **68**, 085318 (2003).
[26]B. S. Mendoza and W. L. Mochán, Opt. Mater. **29**, 1 (2006).
[27]V. L. Brudny, W. L. Mochán, J. A. Maytorena, and B. S. Mendoza, Phys. Status Solidi B **240**, 518 (2003).
[28]D. Östling, P. Stampfli, and K. H. Bennemann, Z. Phys. D **28**, 169 (1993).
[29]J. P. Dewitz, W. Hübner, and K. H. Bennemann, Z. Phys. **37**, 75 (1996).
[30]Y. Pavlyukh and W. Hübner, Phys. Rev. B **70**, 245434 (2004).
[31]A. G. F. de Beer and S. Roke, Phys. Rev. B **79**, 155420 (2009).
[32]S. Roke, M. Bonn, and A. V. Petukhov, Phys. Rev. B **70**, 115106 (2004).
[33]G. Gonella and H.-L. Dai, Phys. Rev. B **84**, 121402 (2011).
[34]*Light Scattering: Principles and Development*, Monographs on the Physics and Chemistry of Materials No. 53, edited by W. Brown (Oxford University Press, Oxford, 1996).
[35]J. Martorell, R. Vilaseca, and R. Corbalán, Phys. Rev. A **55**, 4520 (1997).
[36]S. Roke, W. G. Roeterdink, J. E. G. J. Wijnhoven, A. V. Petukhov, A. W. Kleyn, and M. Bonn, Phys. Rev. Lett. **91**, 258302 (2003).
[37]A. G. F. de Beer and S. Roke, Phys. Rev. B **75**, 245438 (2007).
[38]A. G. F. de Beer, S. Roke, and J. I. Dadap, J. Opt. Soc. Am. B **28**, 1374 (2011).
[39]S. Viarbitskaya, V. Kapshai, P. van der Meulen, and T. Hansson, Phys. Rev. A **81**, 053850 (2010).
[40]G. Mie, Ann. Phys. **330**, 377 (1908).
[41]J. A. Stratton, *Electromagnetic Theory* (McGraw-Hill, New York, 1941).
[42]J. V. Dave, IBM J. Res. Dev. **13**, 302 (1969).
[43]W. J. Wiscombe, Appl. Opt. **19**, 1505 (1980).
[44]W. J. Lentz, Appl. Opt. **15**, 668 (1976).
[45]D. W. Mackowski, R. A. Altenkirch, and M. P. Menguc, Appl. Opt. **29**, 1551 (1990).
[46]O. B. Toon and T. P. Ackerman, Appl. Opt. **20**, 3657 (1981).
[47]C. F. Bohren and D. R. Huffman, *Absorption and Scattering of Light by Small Particles* (Wiley-VCH, New York, 1983).
[48]M. Kerker, *The Scattering of Light and Other Electromagnetic Radiation*, Physical Chemistry No. 16 (Academic, New York, 1969).
[49]A. G. F. de Beer, R. K. Campen, and S. Roke, Phys. Rev. B **82**, 235431 (2010).
[50]V. P. Sokhan and D. J. Tildesley, Mol. Phys. **92**, 625 (1997).
[51]J. H. Bruning and Y. T. Lo, IEEE Trans. Antennas Propag. **AP-19**, 378 (1971).
[52]S. Stein, Q. Appl. Math. **19**, 15 (1961).
[53]B. Schürer, S. Wunderlich, C. Sauerbeck, U. Peschel, and W. Peukert, Phys. Rev. B **82**, 241404 (2010).
[54]B. Schürer, M. Hoffmann, S. Wunderlich, L. Harnau, U. Peschel, M. M. Ballauff, and W. Peukert, J. Phys. Chem. C **115**, 18302 (2011).
[55]G. Wyszecki and W. S. Stiles, *Color Science: Concepts and Methods, Quantitative Data, and Formulae* (Wiley, New York, 2000).
[56]S.-H. Jen, H.-L. Dai, and G. Gonella, J. Phys. Chem. C **114**, 4302 (2010).
[57]S.-H. Jen, G. Gonella, and H.-L. Dai, J. Phys. Chem. A **113**, 4758 (2009).
[58]T. Kikteva, D. Star, and G. W. Leach, J. Phys. Chem. B **104**, 2860 (2000).
[59]N. Yang, W. E. Angerer, and A. G. Yodh, Phys. Rev. Lett. **87**, 103902 (2001).